TOPICS IN CHEMISTRY AND MATERIAL SCIENCE, Vol. 7 (2014) pp. 24–33
Advanced Micro- and Mesoporous Materials – 13
eds. K. Hadjiivanov, V. Valtchev, S. Mintova, G. Vayssilov

Au/Fe_2O_3 Nanocatalysts for Toluene Oxidation as Model VOCs

Z. Bailiche[1,2,5], L. Chérif-Aouali[1], S. Siffert[2,3], S. Royer[4], A. Bengueddach[4]
[1]Laboratoire de Catalyse et Synthèse en Chimie Organique, Université de Tlemcen BP 119, Algérie
[2]Université Lille Nord de France, F-59000 Lille, France
[3]ULCO, UCEIV, F-59140 Dunkerque, France
[4]LACCO, Université de Poitiers-CNRS, ESIP,40 avenue du Recteur Pineau, F-86022 Poitiers cedex, France
[5]Laboratoire de Chimie des Matériaux, Université d'Oran, Algérie

Abstract
Au/ Fe_2O_3 catalysts were synthesized using iron oxide prepared by the nanocasting pathway using the mesoporous SBA-15 silica as structure template and iron nitrate as the Fe_2O_3 precursor via a solid–liquid route.
These catalysts have been characterised by means: H_2-TPR, X-ray powder diffraction (XRD), BET surface area. The gold particles sizes were investigated by high resolution transmission electron microscopy (HRTEM). Catalytic oxidation of toluene was investigated on gold/iron oxide catalysts prepared by deposition-precipitation with different loading of gold (1 wt%, 2 wt%, and 4 wt%). The presence of gold has been found to enhance the activity of iron oxide towards the deep oxidation of toluene, the extent of this effect depending on the gold loading.
The activity for toluene total oxidation of the Au/Fe_2O_3 samples follows this order: 2 wt% $Au/Fe_2O_3 > 4$ wt%$Au/Fe_2O_3 > 1$ wt%Au/Fe_2O_3. The Au/Fe_2O_3 catalysts are active at low temperature and selective for CO_2 and H_2O.
The results we obtained point out that the catalytic activity of the gold/mesoporous iron system towards the deep oxidation of toluene depends on the gold particle size and/or the gold oxidation state and the reducibility of Au_2O_3 to AuO.

1 Introduction

Volatile organic compounds are recognised as major contributors to air pollution, either directly, through their toxic or malodorous nature, or indirectly, as ozone precursors. Many VOCs are health hazards in themselves and can cause cancer or other serious illnesses, even at low concentrations. Industrial processes and transportation activities are mainly responsible for the VOC emissions. Technologies for the removal of VOCs from gas streams can be broadly classified into two groups: those that recover the VOCs for possible later reuse and those that destroy the VOCs [1]. Catalytic oxidation of VOCs is a chemical process

 ISSN 1314–0795

in which hydrocarbons are combined with oxygen at specific temperatures to yield carbon dioxide (CO_2) and water (H_2O). Catalytic oxidation is generally preferred to thermal combustion due to the lower temperature required and to its higher selectivity [2]. Gold has been until recently considered as one of the least catalytically useful metal because of its chemical inertness. However, in the last decade, it has been widely proved that it is possible to prepare gold nanoparticles deposited on metal oxide supports, which exhibit high catalytic activity towards oxidation reactions.

However, despite several reports on gold supported catalysts [3-5], many factors influence the catalytic activity for VOCs type molecule, such as gold loading and oxidation state, gold particle size, nature of the support(reducible or not reducible), calcination temperature. Therefore, a general trend is hard to derive.

Au/Fe_2O_3 [6,7], Au/Al_2O_3 [8]. Au/CeO_2 [9], have been found to have high activities for the decomposition of different kind of VOCs. Gold/iron oxide catalysts revealed a high activity in the catalytic oxidation of toluene and the activity was demonstrated to depend on the extent of interaction between gold-iron nanoclusters supported over titania [10-13]. The catalytic properties of gold catalysts in the oxidation of VOCs have been notably explained by the capacity of small gold particles to increase the mobility of the lattice oxygen in the case of gold supported on ferric oxide [6,14].

In the present work, Au/ Fe_2O_3 catalysts were synthesized using iron oxide prepared by the nanocasting pathway using the mesoporous SBA-15 silica as structure template and iron nitrate as precursor via a solid–liquid route.

The procedure applied resulted in highly active Au/Fe2O3 catalysts for the deep oxidation of toluene: they are active at low temperature and are totally selective for CO_2 and H_2O. 2 wt% Au/Fe_2O_3, the most active catalysts achieves 50% of toluene conversion at 314°C and full toluene conversion at 338°C.

2 Experimental Section

In the present paper, Au/Fe_2O_3 catalysts were synthesized using iron oxide prepared by the nanocasting pathway using the mesoporous SBA-15 silica as structure template and iron nitrate as precursor via a solid–liquid route developed by [14]. If a precursor has a low melting point, when it is simply mixed with a silica template, it may melt before decomposition into another solid phase which has a higher melting point and migrates into the mesopores of silica; decomposition and crystal growth of oxides inside the mesopores will result in mesoporous oxide. This method is solvent-free therefore environmentally friendly.

2.1 Mesoporous materials preparation

Mesoporous SBA15 was synthesized in a way similar to that of Zhao [15]: 4 g of amphiphilic triblock copolymer poly(ethylene oxide)-poly(propylene oxide)-poly(ethylene oxide) (average molecular weight 5800, from Aldrich) was dispersed in 120g of water and 8.64 g of 2M HCl solution at 40°C while stirring followed by the addition of 8.54 g of tetraethyl-orthosilicate (from Aldrich) to

the homogenous solution with stirring. This gel mixture was continuously stirred at 40°C for 24 h, and finally crystallized in a Teflon-lined autoclave at 100°C for 2 days. After cooling to room temperature the solid product was filtered and dried at room temperature in air. Template removal was achieved by calcination in air at 500°C for 4 h (heating rate: 1°C/mn).

Mesoporous iron oxide was synthesized according to the following procedure developed by [14]. One millimole of $Fe(NO_3)_3.9H_2O$ was mixed with 0.15 g of mesoporous silica and was ground for a few minutes in an agate mortar and pestle.

The mix was then put into a crucible, which placed in a muffle furnace. The temperature was increased from room temperature to 500°C at a rate of 1°C/min and maintained at the final temperature for 4H.The specimen was then cooled down to room temperature. The silica template was removed by 2M NaOH solution at 80°C, the porous iron was recovered by centrifugation and washed with distilled water three times.

2.2 Catalysts preparation

The 1 wt%, 2 wt% and 4 wt% Au/Fe_2O_3 catalysts were prepared by deposition-precipitation method: Aqueous solution of tetrachloroauric acid ($HAuCl_4$) (3.65×10^{-4})M was added under stirring to an aqueous suspension of Fe_2O_3 and an aqueous solution of urea (3.65×10^{-3})M in excess. The solution is heated at 80°C to decompose urea and obtain pH = 10. In accordance with the literature data [16], the pH of solution was maintained at the value of 10-11 during 4 h to obtain high dispersion of fine gold particles on the mesoporous iron oxide. The mixture was filtered and washed with deionised water at 60°C several times in order to eliminate the chloride ions, until there were no residual Cl^- ions as tested by $AgNO_3$, dried during 24 h at 80°C and finally calcined under air for 4 h at 400°C.

2.3 Characterization

Powder small- and wide-angle XRD patterns of the calcined samples were recorded on a Bruker AXS D5005 diffractometer equipped with monochromatized Cu Kα radiation ($\lambda = 1.5418$ Å) at 40 kV, 30 mA. Phase identification was performed by comparison with the information of the JCPDS database.

The surface area and pore size analysis of the samples were carried out by adsorption–desorption of nitrogen on a Micromeritics ASAP 2010 instrument (-196°C). Prior to N_2 adsorption, the samples were degassed under vacuum at 250°C for at least 6 h.

The temperature programmed reduction experiments were carried out in an Altamira AMI-200 apparatus.The TPR profiles are obtained by passing a 5% H_2/Ar flow (30 mL/min) through 70 mg of samples heated at 5°C/min from ambient temperature to 800°C. The hydrogen concentration in the effluent was continuously monitored by a thermoconductivity detector (TCD).

The gold particles sizes were investigated by high resolution transmission electron microscopy (HRTEM) using philips CM120 microscope coupled to an

EDX analyser. The average size of the gold particles and the histograms of the particle sizes were performed on 15 images and 280 particles.

Toluene oxidation was carried out in a conventional fixed bed microreactor and studied between 25 and 400°C (1°C/min). The reactive flow was composed of air and 1000ppm of gaseous toluene. The flow rate through the reactor was set at 100 cm^3/min that produced a space velocity of 10000 h^{-1}. The analysis of combustion products was performed evaluating the toluene conversion and the CO/CO+CO_2 molar ratio from a Perkin-Elmer autosystem chromatograph equipped with TCD and FID. Before the catalytic test, the catalyst (100 mg) was calcined under a flow of hydrogen flow (2L h^{-1}) at 200°C (1°C/min).

3 Results and Discussion

3.1 Characterization

XRD. The low-angle XRD patterns of Fe_2O_3 and the Au/Fe_2O_3 catalysts with different gold contents are shown in Figure 1(A). All the patterns exhibit one sharp diffraction corresponding to (100) reflexion which can be associated with the hexagonal symmetry characteristic of mesoporous SBA-15 showing that the ordered structure is maintained in the nanocasting process via a solid–liquid route. No differences on XRD patterns were observed before and after gold

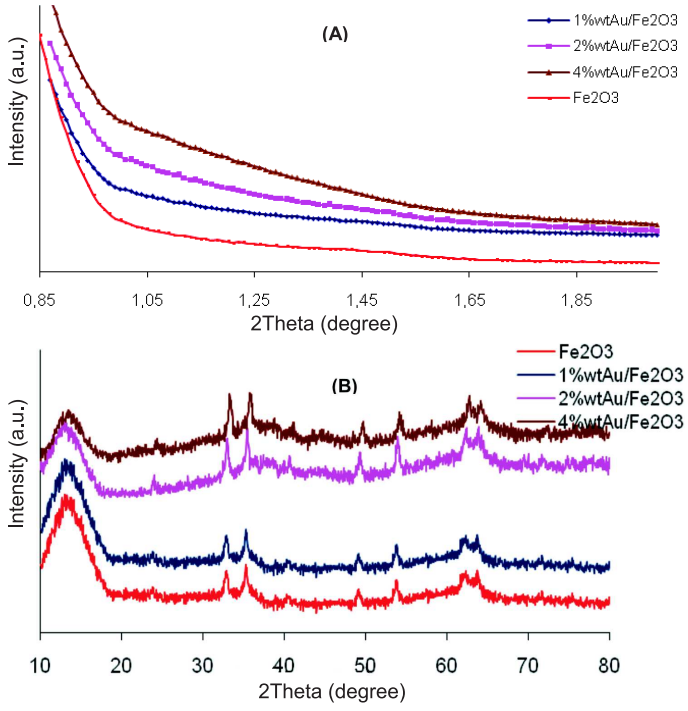

Figure 1. XRD patterns of Fe_2O_3 and the different Au/Fe_2O_3.

deposition suggesting that the introduction of gold does not induce any modification of the support phase. Figure 1(B) shows the wide-angle XRD patterns; On each pattern, the diffraction peaks were perfectly indexed to hematite phase of the Fe_2O_3.

Compared with the diffraction lines of pure mesoporous Fe_2O_3, the catalysts 2 wt% and 4 wt% Au/Fe_2O_3 show a weak diffraction line of gold at $2\theta = 38.5^\circ$ besides the hematite phase of Fe_2O_3.

N_2 adsorption–desorption isotherms. Figure 2 depicts the N_2 adsorption–desorption isotherms of Fe_2O_3 and the Au/Fe_2O_3 catalysts calcined at 400°C. The textural properties of the support and catalysts samples are listed in Table 1.

Table 1. Textural properties of Fe_2O_3 and the Au/Fe_2O_3 catalysts

Sample	S_{BET} (m^2/g)	V_T (cm^{-3}/g)
Fe_2O_3	184	0.4093
1 wt% Au/Fe_2O_3	120	0.3533
2 wt% Au/Fe_2O_3	115	0.3695
4 wt% Au/Fe_2O_3	105	0.2689

X

The isotherms are identified as type IV according to the IUPAC classification, which is a typical characteristic of mesoporous materials [17]. After loading gold particles, the pore volume and the BET surface area decrease with increasing gold content. Generally, when smaller gold particles are dispersed in the pore channels, the channels become narrow, the pore volume decreases and therefore the BET surface area decreases [18].

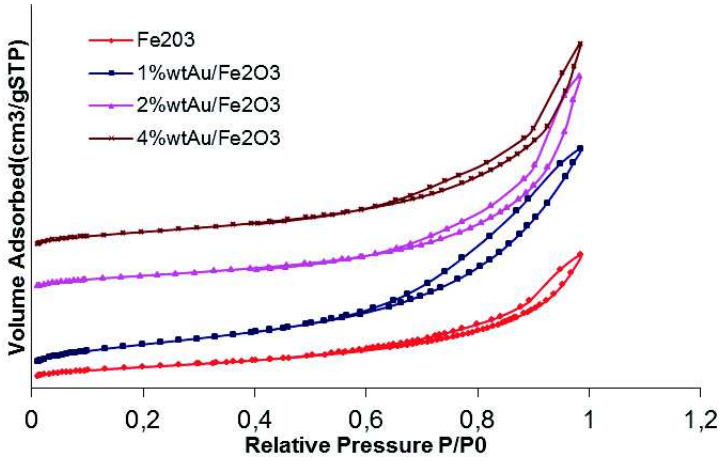

Figure 2. N_2 adsorption-desorption isotherms and BJH pore size distribution of Fe_2O_3 and Au/Fe_2O_3.

TPR. Figure 3 reports temperature programmed reduction (TPR) profiles carried out on Fe_2O_3 and Au/Fe_2O_3 catalysts. The pattern of the Fe_2O_3 sample shows a broad signal starting at a temperature of about 360°C with a maximum at about 575°C. According to the literature [19,20], this signal can be attributed to the reduction of Fe_2O_3 to Fe_3O_4 (magnetite) and to the further transformation of magnetite to FeO. On the other hand, other peaks at lower temperature are found over Au/Fe_2O_3 catalysts. These peaks are attributed to the reduction of Au_xO_y species [21]. Venugopal suggested that the signals appeared at 195 and 232°C are ascribed to the reduction of Au_2O_3 to AuO and AuO to Au respectively [21]. Over 1 wt%, 2 wt% and 4% Au/Fe_2O_3, we suggested that the signals appeared at 203, 82 and 186°C respectively are attributed to the reduction of Au_2O_3 to AuO. A shift in the reduction temperature from 195 to 203, 82 and 186°C indicates that some sort of interaction occurs between Au and the support. Over 2 wt% Au/Fe_2O_3, the signal at 276°C can be attributed to the reduction of AuO to Au.

However, XRD analysis did not reveal the presence of any Au-oxide species. It appears likely therefore that Au_xO_y species are either in low concentration and/or are amorphous and/or are present as very small crystallites. On the sample with the highest metal loading (4 wt% Au/Fe_2O_3) an other signal at higher temperature (638°C) is observed, this peak can be attributed to the transformation of FeO to Fe. Addition of increasing amounts of gold shifts the peak (attributed to $Fe_2O_3 \rightarrow Fe_3O_4 \rightarrow$ FeO) to lower temperature. This means that Au species(oxide or/and metal) strongly influence the reducibility of iron species; This is probably due to the polarization of the Fe-O bonds by Au^{n+} ($n = 1$ or 3), or there may exist synergistic interaction between Au and Fe_2O_3 which result in the easier reduction of Fe_2O_3 species in Au/Fe_2O_3 catalysts; Furthermore Au species in the Au/Fe_2O_3 catalysts could activate H_2; then, the activated H species spillover to the interface of gold, and iron promotes the reduction of Fe oxide species [22].

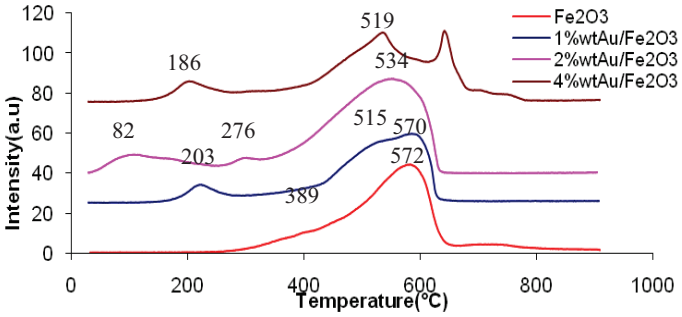

Figure 3. H_2-TPR profiles of Fe_2O_3 and gold- based catalysts.

HRTEM measurements. Figures 4 and 5 show the TEM images and the size histograms of gold particles of the Au/Fe_2O_3 catalysts. The gold particles are seen as dark contrasts on the surface of the support. TEM micrographs show the difference of the average size of the metallic gold particles with the change

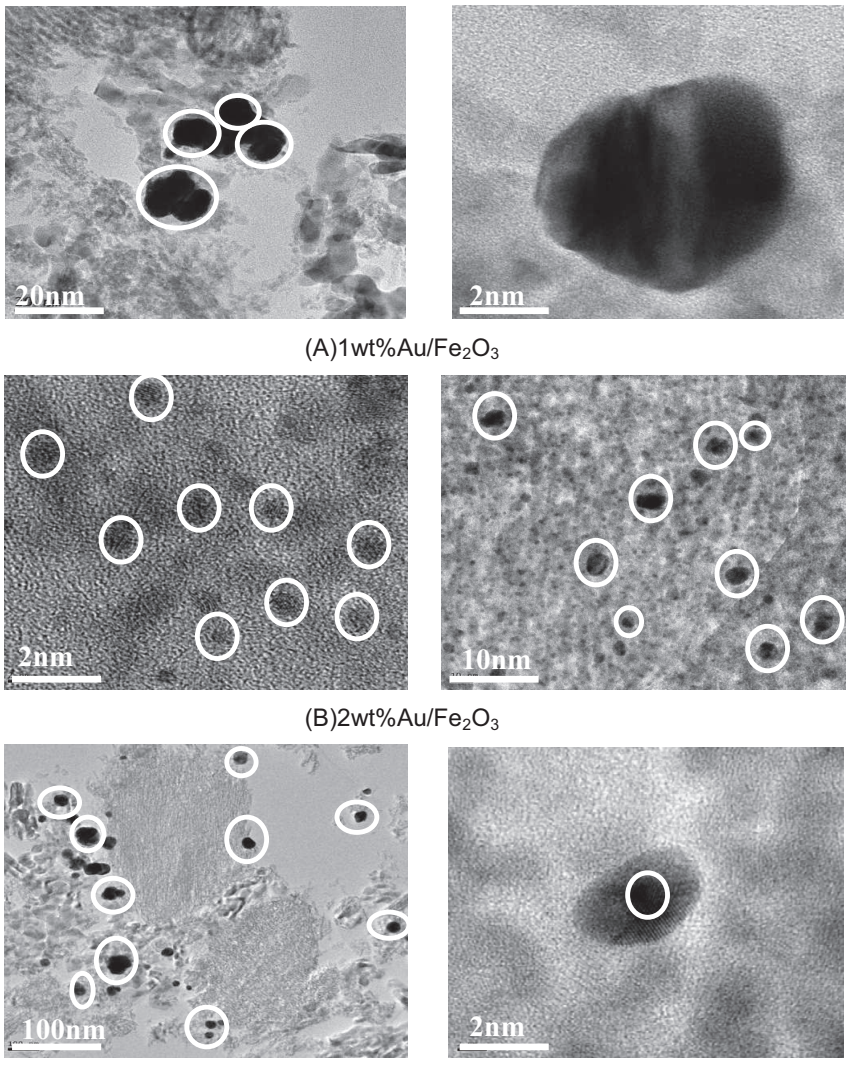

Figure 4. HRTEM images of the $AuCeO_2$ catalysts calcined at 400°C 1 wt% Au/Fe_2O_3, 2 wt% Au/Fe_2O_3, 4 wt% Au/Fe_2O_3.

of gold loading. A homogeneous distribution of gold particles (mean d_{Au}: 4-8nm) is observed on the 2wt% Au/Fe_2O_3 catalyst; Au particles with the diameters less than 2nm are also seen on this catalyst. However the distribution of gold particles on the 1wt% Au/Fe_2O_3 is not uniform (the particle size of gold is between 11and 17nm). Figures 4(C) is the the size histogram of gold particles of 4wt% Au/Fe_2O_3 catalyst. Compared with Figures 4(A) and (B), it can be seen that the particle size of gold in the 4wt% Au/Fe_2O_3 catalyst is bigger than

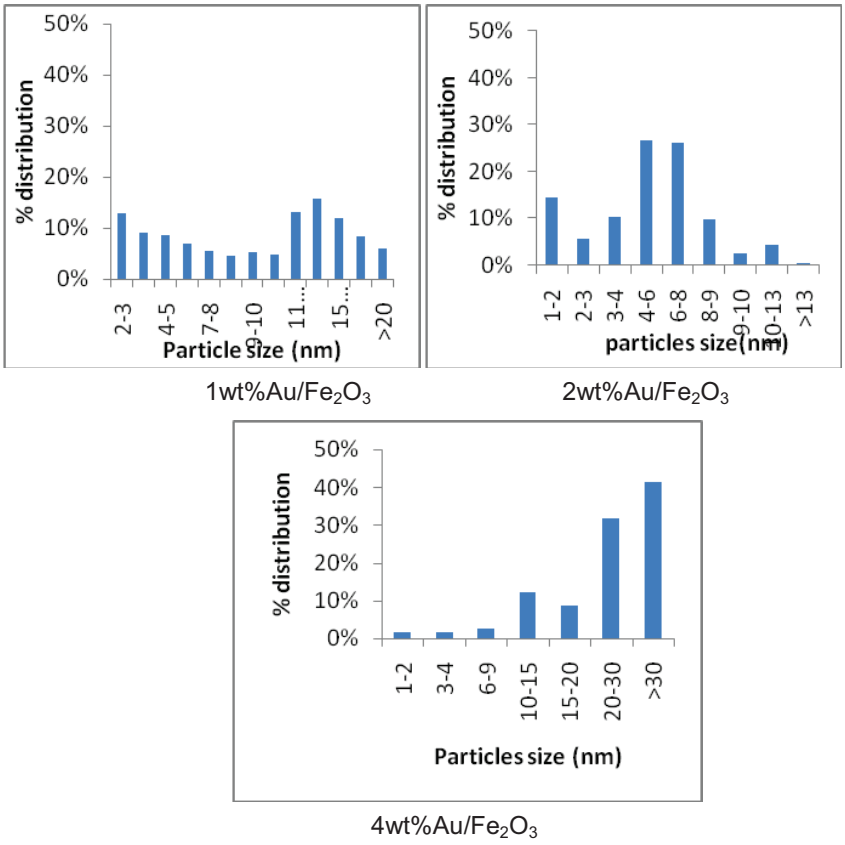

Figure 5. Histograms of gold particles size distribution of the Au/Fe_2O_3.

that in 1wt% Au/Fe_2O_3 and 2wt% Au/Fe_2O_3 and is larger than 20nm.This result demonstrates that the dispersion of the metallic gold particles deposited on the mesoporous iron oxide depends on the gold loading.

3.2 Catalytic activity for total toluene oxidation

Toluene oxidation curves versus temperature are presented in Figure 6. The activity is given by the T_{50} value (temperature for a conversion of 50%) (Table 2).

The observed products are only carbon dioxide and water indicating complete combustion occurring during the reaction.

As shown in Table 2, over Fe_2O_3, 1 wt% Au/Fe_2O_3, 2 wt% Au/Fe_2O_3 and 4 wt% Au/ Fe_2O_3 catalysts, the oxidation of toluene reached 50% of conversion at 362°C, 340°C, 314°C and 325°C respectively. It is worth noting that the T_{50} shift, with respect to pure mesoporous iron oxide, is significant for a gold loading 2 wt%. It is important to note that the oxidation of toluene reached 100% of conversion at 338°C over 2 wt% Au/Fe_2O_3.

Table 2. $T_{50\%}$ values (°C) for toluene oxidation for various Au/Fe_2O_3

Sample	Temperature of toluene conversion $T_{50\%}$ (°C)
Fe_2O_3	362
1 wt% Au/Fe_2O_3	340
2 wt% Au/Fe_2O_3	314
4 wt% Au/Fe_2O_3	325

It must be remind that 2 wt% Au/Fe_2O_3 exhibits the smallest gold particle size and this could explain the highest catalytic activity of this catalyst. Indeed, it has been reported that the activity of gold catalysts towards several reactions increases as the gold particle size decreases [4]. The catalytic properties of gold catalysts in the oxidation of VOCs have been notably explained by the capacity of small gold particles to increase the mobility of the lattice oxygen in the case of gold supported on ferric oxide [6,14]. It is important to note that 4 wt% Au/Fe_2O_3 catalyst, for which the biggest gold particle size has been found, is more active than the 1 wt% Au/Fe_2O_3 catalyst. It must be reminded that the reduction of Au_2O_3 to AuO in 4 wt% Au/Fe_2O_3 is easier than that in 1 wt% Au/Fe_2O_3. It must be also remind that TPR characterization data performed on the Au/Fe_2O_3 catalysts showed that AuO species are present only in the 2 wt% Au/Fe_2O_3 sample, the most active catalyst.

The results we obtained point out that gold active species are Au^0 and Au^{n+} ($n = 1$ or 3) in the deep oxidation of toluene over gold/mesoporous iron oxide system and the catalytic activity depends on the gold particle size and/or the gold oxidation state and the reducibility of Au_2O_3 to AuO.

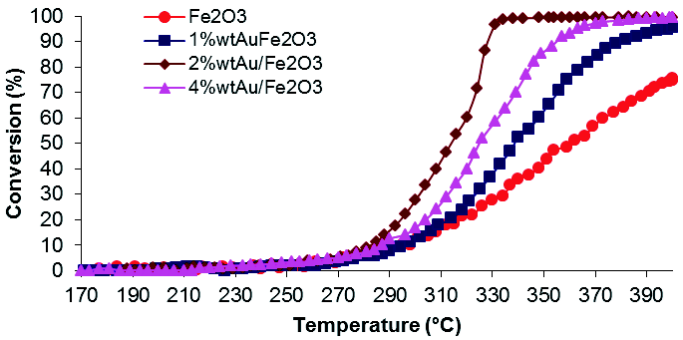

Figure 6. Toluene conversion on Fe_2O_3 and gold- based catalysts.

4 Conclusion

The Au/Fe_2O_3 catalysts are found to be highly active catalysts for deep oxidation of toluene. They are active at low temperature and selective for CO_2 and H_2O. The activity for toluene total oxidation of the Au/Fe_2O_3 samples follows this

order: 2 wt% Au/ Fe_2O_3 > 4 wt% Au/Fe_2O_3 > 1 wt% Au/Fe_2O_3.

Our results point out that the catalytic activity of the gold/mesoporous iron oxide system towards the deep oxidation of toluene depends on the gold particle size and/or the gold oxidation state and the reducibility of Au_2O_3 to AuO.

References

[1] F. Wyrwalsky, J.-F. Lamonier, S. Siffert, A. Aboukaïs, *Appl. Catal. B* **70** (2007) 393-399.

[2] E.C. Moretti, N. Mukhopadhyay, *Chem. Eng. Prog.* **89** (1993) 20-26.

[3] G.C. Bond, C. Louis, D.T. Thompson, "*Catalysis by Gold*" (Imperial College Press, London, 2006).

[4] G.C. Bond, D.T. Thompson, *Catal. Rev. Sci. Eng.* **41** (1999) 319.

[5] M.S. Chen, D.W. Goodman, *Acc. Chem. Res.* **39** (2006)739-746.

[6] S. Minico, S. Scire, C. Crisafulli, R. Maggiore, S. Galvagno, *Appl. Catal., B* **28** (2000) 245-251.

[7] S. Minico, S. Scire, C. Crisafulli, S. Galvagno, *Appl. Catal., B* **34** (2001) 277-285.

[8] R.M. Finch, N.A. Hodge, G.J. Hutchings, A. Meagher, Q.A. Pankhurst, S. Scire, S. Minico, C. Crisafulli, S. Galvagno, *Catal. Commun.* **2** (2001) 229-232.

[9] M.A. Centeno, M. Paulis, M. Montes, J.A. Odriozola, *Appl. Catal., A* **234** (2002) 65-78.

[10] M.L. Jia, H.F. Bai Zhaorigetu, Y.N. Shen, Y.F. Li, *J. Rare Earths* **26** (2008) 528-531.

[11] B. Solsona, T. Garcia, R. Murillo, A.M. Mastral, E.N. Ndifor, C.E. Hetrick, M.D. Amiridis, S.H. Taylor, *Top. Catal.* **52** (2009) 492-500.

[12] S. Scire, S. Minico, C. Crisafulli, C. Satriano, A. Pistone, *Appl. Catal., B* **40** (2003) 43-49.

[13] D. Andreeva, P. Petrova, J.W. Sobczak, L. Ilieva, M. Abrashev, *Appl. Catal., B* **67** (2006) 237-245.

[14] W.Yue, W. Zhou, *Chem. Mater.* **19** (2007) 2359-2363.

[15] D. Zhao, J. Feng, Q. Huo, N. Melosh, G.H. Frederickson, B.F. Chmelka, G. D. Stucky, *Science* **279** (1998) 548-552.

[16] D.M. Lyons, J.P. McGrath, M.A. Morris, *J. Phys. Chem. B* **107** (2003) 4607.

[17] K.S.W. Sing, D.H. Everett, R.A.W. Haul, L. Moscou, R.A. Pierotti, J. Rouquerol, T. Siemieniewska, *Pure Appl. Chem.* **57** (1985) 603-619.

[18] L. Qian, M. Ming, Z. Yuqing, *Chin. J. Catal.* **27** (2006) 1111-1116.

[19] G. Neri, A.M. Visco, S. Galvagno, A. Donato, M. Panzalorto, *Thermochim. Acta* **329** (1999) 39-46.

[20] G. Munteanu, L. Ilieva, D. Andreeva, *Thermochim. Acta* **291** (1997) 171-177.

[21] A. Venugopal, M.S. Skurrell, *Appl. Catal., A* **258** (2004) 241-249.

[22] G.Y. Wang, H.L. Lian, W.X. Zhang, D.Z. Jiang, T.H. Wu, *Kinet. Catal.* **43** (2002) 433-442.